ACS Energy LETTERS

http://pubs.acs.org/journal/aelccp

LETTER

Direct X-ray Detectors Based on an Eco-Friendly Semiconducting Zero-Dimensional Organic Zinc Bromide Hybrid

Oluwadara J. Olasupo, Thanh-Hai Le, Tunde B. Shonde, He Liu, Alexander Bouchard, Sara Bouchard, Thilina N. D. D. Gamaralalage, Abiodun M. Adewolu, Tarannuma F. Manny, Xinsong Lin, Yan-Yan Hu, Wanyi Nie,* and Biwu Ma*

Cite This: *ACS Energy Lett.* 2024, 9, 5704−5711

Read Online

ACCESS | Metrics & More | Article Recommendations | Supporting Information

ABSTRACT: **Direct X-ray detectors that convert X-rays to electrical charges have broad applications in medicine and security screening. Common semiconductors like silicon and selenium for direct X-ray detectors have limitations in performance, versatility, and cost-effectiveness. Among new materials under investigation, metal halide perovskites demonstrate great potential for X-ray detectors; however, they are limited by low stability and toxicity. Here, we report, for the first time, a stable and eco-friendly zero-dimensional (0D) organic metal halide hybrid (OMHH), $(TPA\text{-}P)_2ZnBr_4$, for efficient X-ray detectors. With molecular sensitization, wherein metal halides ($ZnBr_4^{2-}$) act as X-ray absorbers and organic semiconducting components (TPA-P$^+$, 4-(4-(diphenylamino)phenyl)-1-propylpyridin-1-ium) as charge transporters, 0D $(TPA\text{-}P)_2ZnBr_4$ detectors exhibit an impressive sensitivity of 2,292 $\mu C\ Gy_{air}^{-1}\ cm^{-2}$ at 20 V and a low detection limit of 37.5 $nGy_{air}\ s^{-1}$. The exceptional stability of 0D $(TPA\text{-}P)_2ZnBr_4$ facilitates remarkably stable direct X-ray detection and shows the tremendous potential of rationally designed 0D OMHHs as new-generation radiation detection materials.**

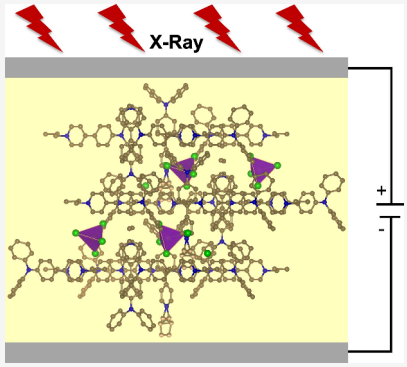

Since the groundbreaking discovery of X-rays by Wilhelm C. Röntgen in 1895,[1] our world has continued to benefit from it in numerous aspects, from healthcare to security, scientific research, and industrial processes. Thanks to X-ray detectors developed over the years, X-ray imaging has been utilized for medical diagnostics like radiography and CT scans, homeland security screening, and many other applications.[2−6] To date, most commercially available direct X-ray detectors being used to convert X-rays into electrical signals are constructed with inorganic semiconductors, such as amorphous silicon and selenium.[7,8] However, direct X-ray detectors based on pure inorganic semiconductors have many disadvantages, including cost, bulkiness, temperature sensitivity, radiation damage, and energy dependency.[9] Because of these limitations, semiconductor detectors are still behind other sensing technologies for wide adoption in the market. In recent years, researchers have explored new types of materials for direct X-ray detectors, for instance, metal halide perovskites and perovskite-related hybrid materials.[3,10−15] Stoumpos et al. reported direct radiation detectors based on $CsPbBr_3$ in 2013,[10] which exhibited a high linear attenuation coefficient of about 1 μm^{-1} at a photon energy range of 1−1000 keV and a large carrier mobility lifetime product of $1.7 \times 10^{-3}\ cm^2\ V^{-1}$, significantly higher than that of α-Se ($\sim 10^{-7}\ cm^2\ V^{-1}$).[16] Pan et al. also demonstrated X-ray detectors based on lead-free double-perovskite $Cs_2AgBiBr_6$,[17] which exhibited high resistivities ranging from 10^9−$10^{11}\ \Omega$ cm, a large carrier mobility lifetime product of $6.3 \times 10^{-3}\ cm^2 \cdot V^{-1}$, and a low limit of detection of around 59.7 $nGy_{air}\ s^{-1}$. Despite many high figure-of-merits of perovskite-based detectors, metal halide perovskites with a 3D structure at the molecular level possess high charge carrier concentrations and exhibit high dark current due to unintentional self-doping effects.[18−24] Moreover, they often suffer from low stability, especially when exposed to moisture with water molecules that easily penetrate the crystal structure to weaken bonding interactions between metal halide polyhedral and small organic cations. This leads to free ionic migration and fast degradation.[25−27] To address both high dark current and stability issues, researchers have looked into lower dimensional materials with suppressed self-doping effects and

Received: September 26, 2024
Revised: October 22, 2024
Accepted: October 28, 2024
Published: November 1, 2024

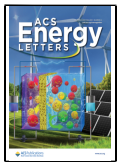

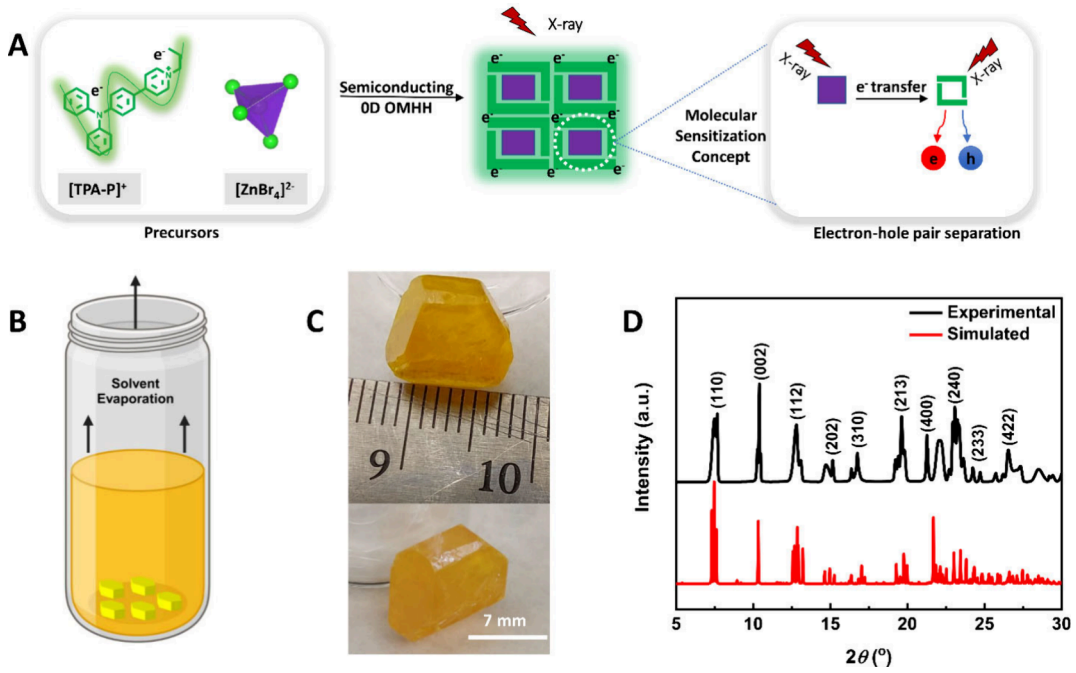

Figure 1. Material design concept, growth, and characterization of 0D $(TPA\text{-}P)_2ZnBr_4$ single crystals. (a) Schematic diagram of the molecular sensitization of 0D $(TPA\text{-}P)_2ZnBr_4$, where $ZnBr_4^{2-}$ acts as X-ray absorbers and interconnecting $TPA\text{-}P^+$ serves as the charge transporters. (b) Schematic illustration of the slow room temperature evaporation of a precursor solution of 2:1 molar ratio of TPA-PBr and $ZnBr_2$ to grow large crystals of 0D $(TPA\text{-}P)_2ZnBr_4$ (Created with BioRender.com). (c) Top and side views of a 0D $(TPA\text{-}P)_2ZnBr_4$ single crystal. (d) Powder X-ray diffraction patterns of 0D $(TPA\text{-}P)_2ZnBr_4$ showing well-matched peaks with simulation results.

reduced carrier concentrations, including 2-dimensional (2D), 1D, and 0D organic metal halide hybrids (OMHHs), where the steric effects introduced by bulky organic cations could minimize ion migration and increase the defect formation energy.[20,23,28−30]

0D OMHHs, containing metal halide anions fully isolated and surrounded by organic cations, have recently emerged as a new class of functional materials with a wide range of applications, such as down-conversion emitters and X-ray scintillators.[31−35] The site isolation of metal halides by organic cations in 0D OMHHs grants them significantly greater stability when compared to 3D metal halide perovskites. This characteristic also endows them with substantial potential to achieve minimal current drift by effectively suppressing ionic migration.[15] Liu et al. reported the use of 0D $(MA)_3Bi_2I_9$ for X-ray detectors, which exhibited a low dark current of around 8 pA (electric field ~10 V mm^{-1}).[15] You et al. reported a self-driven X-ray detector based on chiral 0D $(R/S\text{-}PPA)_2BiI_5$, showing a low dark current density (~80 pA cm^{-2} at zero bias).[36] Although excellent photocurrent stability with low dark currents has been achieved in these 0D OMHHs-based X-ray detectors,[15,36] the low conductivity of 0D OMHHs due to the insulating nature of organic cations used in these materials leads to low sensitivity. To facilitate the use of 0D OMHHs in direct X-ray detectors, it is crucial to tackle the low electrical conductivity characteristic of existing OMHHs containing insulating organic cations. This could be achieved by developing 0D OMHHs that contain semiconducting organic cations.

Here, we report, for the first time, the use of a single crystalline 0D OMHH containing semiconducting organic cations, 0D $(TPA\text{-}P)_2ZnBr_4$, for the fabrication of high-performance direct X-ray detectors, where $TPA\text{-}P^+$ represents 4-(4-(diphenylamino)phenyl)-1-propylpyridin-1-ium with a bandgap of 2.25 eV. By integrating wide bandgap $ZnBr_4^{2-}$ anions with bulky semiconducting $TPA\text{-}P^+$ cations, we achieved a 0D $(TPA\text{-}P)_2ZnBr_4$ with highly efficient molecular sensitization, where electrons can be ionized in the $ZnBr_4^{2-}$anions upon X-ray irradiation and transferred to semiconducting $TPA\text{-}P^+$ organic cations for charge conduction. Subsequently, 0D $(TPA\text{-}P)_2ZnBr_4$-based direct X-ray detectors are fabricated to exhibit an impressive sensitivity of 2,292 $\mu C\ Gy_{air}^{-1}\ cm^{-2}$ at 20 V bias with a low detection limit of 37.5 $nGy_{air}\ s^{-1}$. Electronic characterizations have revealed a low trap density of $2.86 \times 10^9\ cm^{-3}$ and a high mobility lifetime product of $5.67 \times 10^{-4}\ cm^2\ V^{-1}$ at 20 V for 0D $(TPA\text{-}P)_2ZnBr_4$ single crystals. The high resistivity of $5.05 \times 10^{10}\ \Omega$ cm of 0D $(TPA\text{-}P)_2ZnBr_4$ is crucial in realizing a very low and stable average dark current of around 13.4 pA under 24 h of operation.

In 2023, our group reported the application of 0D $(TPA\text{-}P)_2ZnBr_4$ for high-performance X-ray scintillation, where metal halides $ZnBr_4^{2-}$ act as sensitizers with high X-ray absorption and aggregation-induced emission (AIE) organic cations $TPA\text{-}P^+$ act as efficient light emitters with a short decay lifetime of 3.52 ns.[33] Considering the semiconducting nature of $TPA\text{-}P^+$ with a bandgap of 2.25 eV, we believe that 0D $(TPA\text{-}P)_2ZnBr_4$ could also be used to fabricate direct X-ray detectors. Figure 1A shows the concept of molecular sensitization of 0D $(TPA\text{-}P)_2ZnBr_4$ for direct X-ray detectors, where $ZnBr_4^{2-}$ serves as the main X-ray absorber and $TPA\text{-}P^+$ as the charge transporter. In other words, instead of reading visible light output from $TPA\text{-}P^+$ in 0D $(TPA\text{-}P)_2ZnBr_4$-based X-ray scintillators, direct detection of electrical signals can be achieved in 0D $(TPA\text{-}P)_2ZnBr_4$-based direct X-ray detectors. Indeed, the molecular sensitization approach offers tremendous potential in enhancing the performance of direct X-ray detectors. First, it enables high X-ray detection sensitivity by using metal halides with

https://doi.org/10.1021/acsenergylett.4c02662
ACS Energy Lett. 2024, 9, 5704−5711

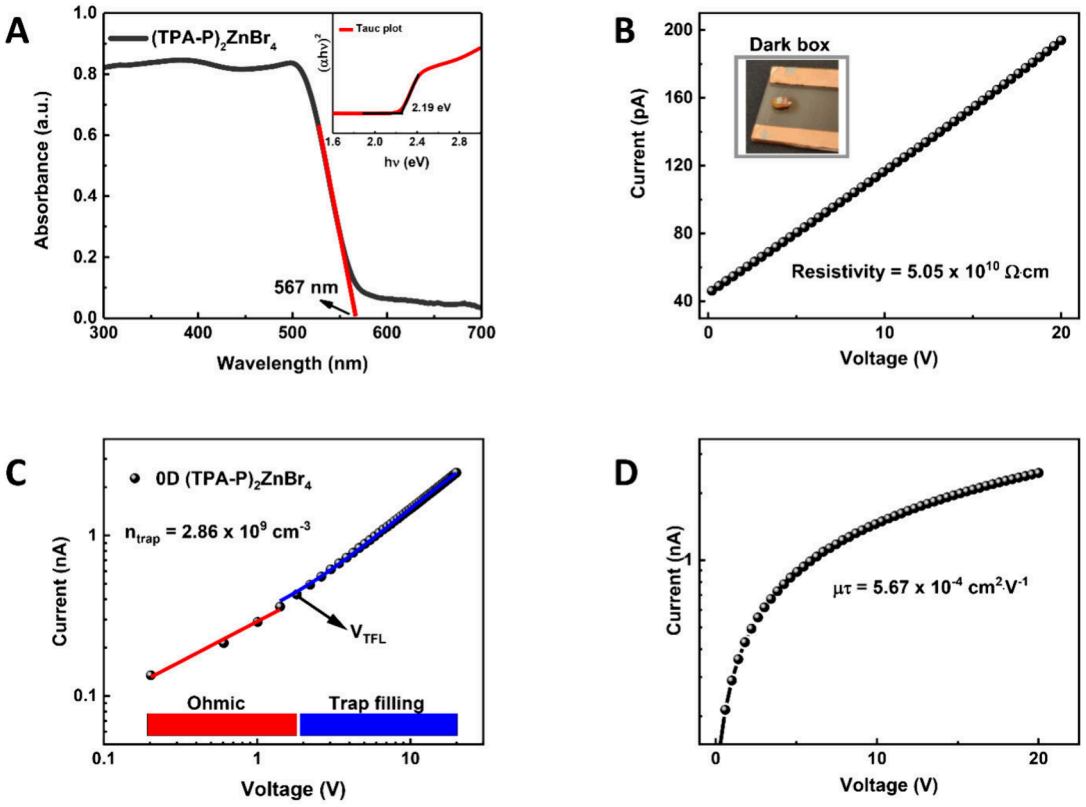

Figure 2. Photophysical and electronic characterizations of 0D $(TPA\text{-}P)_2ZnBr_4$. (a) Ultraviolet-visible solid-state absorptance spectrum of 0D $(TPA\text{-}P)_2ZnBr_4$ with an estimated bandgap of 2.19 eV shown in the inset. (b) I−V plot showing the dark resistivity of a 1.2 mm thick 0D $(TPA\text{-}P)_2ZnBr_4$ crystal in a vertical device shown in the inset. (c) Dark I−V curve fitting under the space charge-limited current (SCLC) model. (d) Bias-dependent photoconductivity of a 0D $(TPA\text{-}P)_2ZnBr_4$-based detector under continuous X-ray irradiation.

strong X-ray absorption to sensitize lightweight semiconducting organic molecules. Unlike previous blended systems that combine high atomic weight metal nanoparticles with organic polymers, often hampered by issues of film uniformity and poor air stability,[37,38] molecular sensitization in 0D OMHHs relies on single crystals with highly ordered molecular structures. These crystalline structures provide improved uniformity, air stability, and more efficient energy transfer processes,[33] resulting in superior X-ray detection performance. Additionally, incorporating molecular sensitization into 0D OMHHs opens up opportunities for molecular design and engineering. By selecting organic molecules with excellent charge carrier mobilities, the electrical conductivity and sensitivity of X-ray detectors can be further enhanced.

To obtain large single crystals of 0D $(TPA\text{-}P)_2ZnBr_4$ for the fabrication of direct X-ray detectors, we have slightly changed the crystal growth method from the previously used antisolvent diffusion growth to a slower room temperature evaporation method, as shown in Figure 1B. More specifically, a precursor solution was prepared by dissolving TPA-PBr and $ZnBr_2$ in dimethylformamide (DMF) at a 2:1 mol ratio, respectively, which was filtered and placed in a large vial and gently left open at room temperature to achieve gradual evaporation of the solvent (Figure S1). 0D $(TPA\text{-}P)_2ZnBr_4$ single crystals started to appear after 48 h and hexagonal-shaped single crystals with size dimensions of up to 7 mm × 3 mm × 2 mm (Figure 1C) could be prepared with excellent surface smoothness after around 1 week. The structure and composition of large size 0D $(TPA\text{-}P)_2ZnBr_4$ single crystals were confirmed to be the same as those of smaller single crystals previously prepared using the antisolvent diffusion growth method,[33] with SCXRD data shown in Table S1. The powder X-ray diffraction (PXRD) patterns of powder samples obtained from large-size single crystals match perfectly with the simulated ones from single-crystal XRD, suggesting the high purity of the large single crystals. The thermal stability test, conducted using thermogravimetric analysis (TGA) (Figure S2), indicates that the material remains stable and does not decompose until approximately 300 °C.

The basic optical and electronic properties of large-size 0D $(TPA\text{-}P)_2ZnBr_4$ single crystals have been characterized. Figure 2A shows the absorption spectrum of 0D $(TPA\text{-}P)_2ZnBr_4$ single crystals with an absorption edge cutoff at around 567 nm, from which the optical bandgap is estimated to be around 2.19 eV. TPA-PBr shows a similar bandgap of around 2.25 eV as determined by cyclic voltammetry (Figure S3 and Table S2) and UV−vis absorption spectroscopy (Figure S4). The slightly decreased bandgap of 0D $(TPA\text{-}P)_2ZnBr_4$ as compared to TPA-PBr is likely due to the enhanced molecular packing of $TPA\text{-}P^+$ cations in 0D $(TPA\text{-}P)_2ZnBr_4$ single crystals.[33] The resistivity of 0D $(TPA\text{-}P)_2ZnBr_4$ single crystals with a thickness of 1.2 mm in the dark was determined to be around 5.05×10^{10} Ω cm using a simple vertical two-terminal measurement as shown in Figure 2B (see the experimental details in the methods section of the Supporting Information), which is three orders of magnitude higher than those of typical 3D $MAPbX_3$ (X = Cl, Br, I) perovskites single crystals,[19] and similar to those of recently reported 0D $MA_3Bi_2I_9$ (3.75×10^{10} Ω cm) and 0D $(R/S\text{-}PPA)_2BiI_5$ (2.96×10^{10} Ω cm).[15,36]

https://doi.org/10.1021/acsenergylett.4c02662
ACS Energy Lett. 2024, 9, 5704−5711

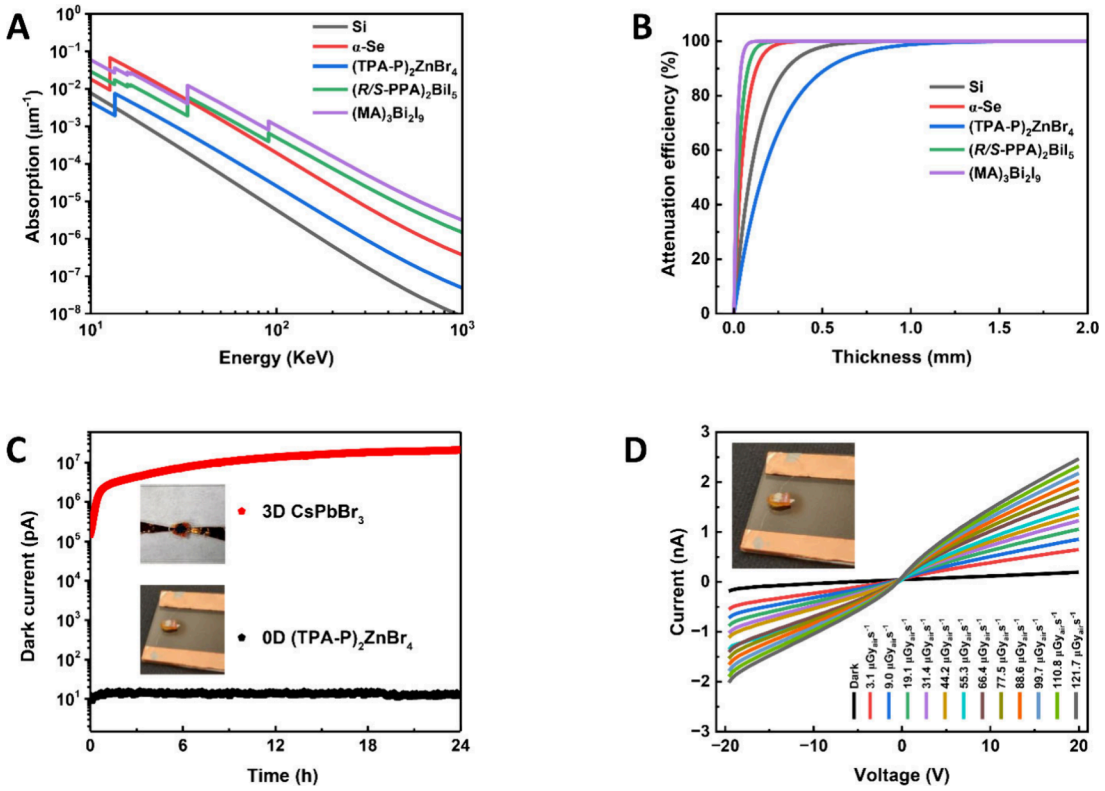

Figure 3. The X-ray detection performance of 0D $(TPA\text{-}P)_2ZnBr_4$ device. (a) Calculated X-ray absorption coefficients versus photon energy for 0D $(TPA\text{-}P)_2ZnBr_4$ compared to α-Se, Si, and a few reported 0D OMHHs. (b) X-ray attenuation efficiency of the different detectors under 10.3 keV X-ray energy versus required detector thickness. (c) Dark current versus time plots compared for both 3D $CsPbBr_3$ and 0D $(TPA\text{-}P)_2ZnBr_4$ detectors with insets of both devices. (d) I–V plot showing X-ray detection results of 0D $(TPA\text{-}P)_2ZnBr_4$ at 20 V from dark to X-ray dose rate of 121.7 $\mu Gy_{air}\ s^{-1}$.

We have further determined the trap density n_{trap} of 0D $(TPA\text{-}P)_2ZnBr_4$ single crystal using the space charge-limited current (SCLC) method at a bias of 20 V. After fitting the dark I–V under the SCLC model as shown in Figure2C, two distinct regimes corresponding to $I \propto V^n$ were identified, where $n = 1$ and $n > 2$ are ascribed to Ohmic and Trap-Filling Limited (TFL) regimes, respectively. The trap density n_{trap} was then calculated by using eq 1

$$n_{trap} = \frac{2V_{TFL}\varepsilon\varepsilon_0}{eL^2} \tag{1}$$

where V_{TFL} is the trap-fill voltage marking the transition from the Ohmic regime to the TFL regime of the I–V plot (1.82 V), ε_0 is the vacuum permittivity (8.854×10^{-12} F m^{-1}), ε is the permittivity obtained from the Capacitance vs Frequency data plot in Figure S5, e is the elementary charge of 1.602×10^{-19} C, and L is the thickness of the sample (1.2 mm).[39,40] The obtained n_{trap} value of 2.86×10^9 cm^{-3} is much lower than those of 2D and 3D halide perovskites, and comparable to those of 0D OMHHs.[13,40,41] To evaluate the potential of 0D $(TPA\text{-}P)_2ZnBr_4$ single crystals for direct X-ray detection, we have determined the carrier mobility lifetime product $\mu\tau$, which is an important parameter characterizing the carrier collection efficiency. Under continuous X-ray irradiation of 121.7 $\mu Gy_{air}\ s^{-1}$, the voltage-dependent photoconductivity of 0D $(TPA\text{-}P)_2ZnBr_4$ single crystal, $\mu\tau$ was estimated to be 5.67×10^{-4} $cm^2 \cdot V^{-1}$ (Figure 2D) according to the Modified Hecht eq 2[42]

$$I = \frac{I_0\mu\tau V}{L^2}\left[1 - \exp\left(\frac{-L^2}{\mu\tau V}\right)\right] \tag{2}$$

where L represents the thickness of the sample between two electrodes, and I_0 represents the saturated photocurrent reached under voltage bias V. It is found that the $\mu\tau$ of 0D $(TPA\text{-}P)_2ZnBr_4$ is three orders of magnitude higher than that of α-Se (10^{-7} cm^2 V^{-1}) and is comparable to 0D $Cs_3Bi_2I_9$ (7.97×10^{-4} cm^2 V^{-1}).[16,40] All the electrical characterization results of 0D $(TPA\text{-}P)_2ZnBr_4$ single crystals, i.e. a low trap density of 2.86×10^9 cm^{-3} and a high carrier mobility lifetime product of 5.67×10^{-4} cm^2 V^{-1}, confirm the effectiveness of our molecular design of 0D OMHHs containing bulky semiconducting organic cations for direct X-ray detectors.

The theoretical X-ray absorption coefficient of 0D $(TPA\text{-}P)_2ZnBr_4$ within a range of practical photon energies from 10 to 1000 keV was calculated using a photon cross-section database, as shown in Figure 3A.[43] It is found that 0D $(TPA\text{-}P)_2ZnBr_4$ with a density of 1.54 g cm^{-3} has a slightly lower absorption coefficient than those of α-Se (4.25 g cm^{-3}) and 0D bismuth halide hybrids, such as $MA_3Bi_2I_9$ (4.11 g cm^{-3}) and $(R/S\text{-}PPA)_2BiI_5$ (2.51 g cm^{-3}).[15,16,36,44] Figure 3B shows the attenuation efficiency versus thickness plots for 0D $(TPA\text{-}P)_2ZnBr_4$ and several known X-ray detection materials. A thickness of around 1.1 mm is needed for 0D $(TPA\text{-}P)_2ZnBr_4$ single crystals to achieve near-unity attenuation at 10.3 keV energy, which is not surprising considering the relatively low Z compositions of 0D $(TPA\text{-}P)_2ZnBr_4$ as compared to those of other materials. On the other hand, our material can be

https://doi.org/10.1021/acsenergylett.4c02662
ACS Energy Lett. 2024, 9, 5704−5711

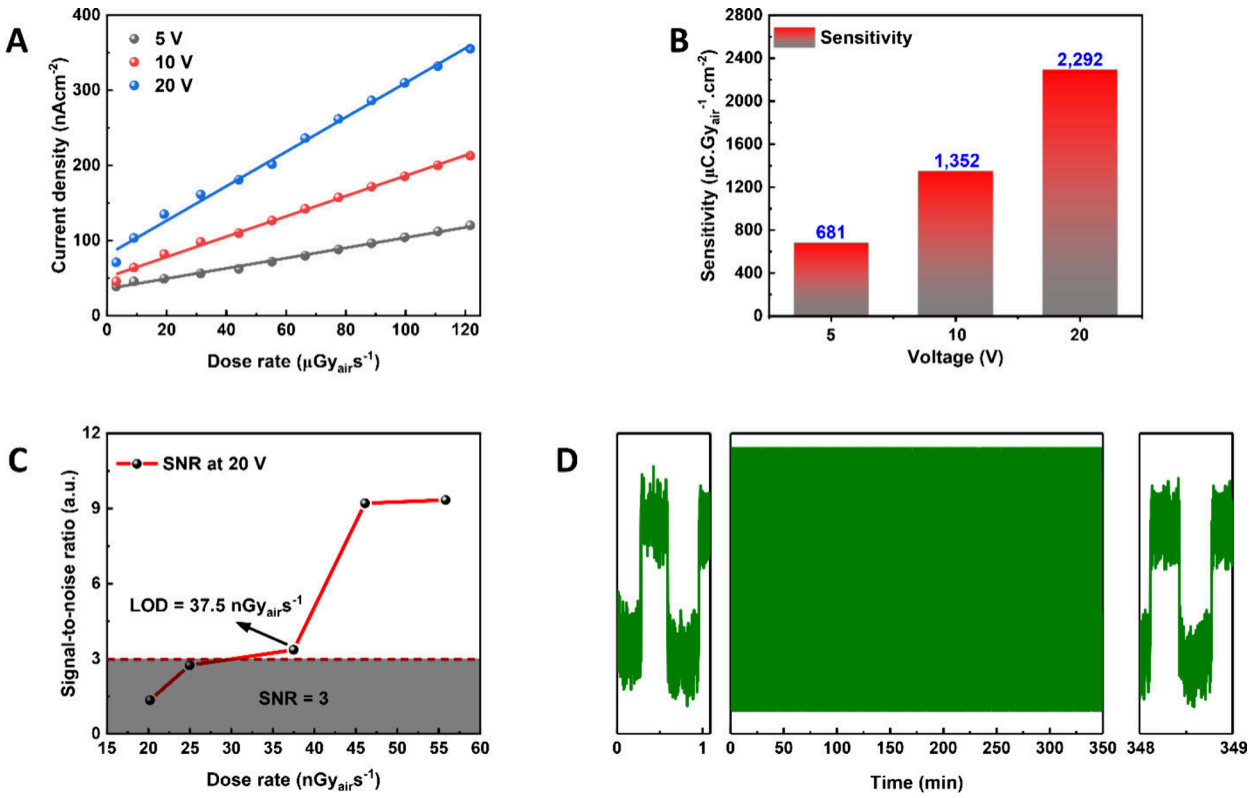

Figure 4. Extended X-ray detection performance and long-term operational stability test of 0D (TPA-P)$_2$ZnBr$_4$ device. (a) X-ray current density as a function of dose rate under different applied bias voltages. (b) X-ray sensitivity of 0D (TPA-P)$_2$ZnBr$_4$ detector as a function of varying bias voltages. (c) The signal-to-noise ratio (SNR) of 0D (TPA-P)$_2$ZnBr$_4$ detector was obtained by measuring the X-ray current signals and the standard deviation of the respective X-ray currents measured at various dose rates. The detection limit of 37.5 nGy$_{air}$ s^{-1} at 20 V corresponds to the signal at an SNR of 3.36. (d) 580 complete on-off cycles response of our detector performed under an X-ray dose of 178.7 μGy$_{air}$ s^{-1} at 20 V (on time: 20 s, off time: 20 s).

upscaled to the volume needed for the desired attenuation at a low cost.

Direct X-ray detectors based on 0D (TPA-P)$_2$ZnBr$_4$ were fabricated using a vertical photoconductor architecture with single crystals of around 1.1 mm thick sandwiched between a pair of silver electrodes, as shown in the inset of Figure 3C. We have compared the performance of devices based on 0D (TPA-P)$_2$ZnBr$_4$ single crystals to a control device based on a 3D $CsPbBr_3$ single crystal. As shown in Figure 3C, devices based on 0D (TPA-P)$_2$ZnBr$_4$ possess an average dark current of around 13 pA under 5 V bias, which is significantly lower than that of $CsPbBr_3$-based devices averaged at 14 μA when driven at the same bias. Moreover, the dark current of devices based on 0D (TPA-P)$_2$ZnBr$_4$ remains largely unchanged during continuous operation for over 24 h.[45] In contrast, the devices based on 3D $CsPbBr_3$ single crystals undergo significant drifting, where the dark current increases by almost 100 times after 24 h of voltage stress in the dark. This dark baseline drifting is likely attributed to the voltage-induced ion migrations in 3D perovskites, where mobile ions can create conducting channels through the surface with increased dark currents.[25,46] In OMHHs with reduced dimensionalities, the steric hindrance of large organic cations has been shown to suppress defect formation with an ultralow self-doping, resulting in a significantly suppressed ion migration and dark current, which is highly desired for radiation detectors.[19,20,23]

We have further characterized the X-ray detection performance of devices based on 0D (TPA-P)$_2$ZnBr$_4$ with an electrode area of 0.8 × 0.8 mm^2 at various radiation dose rates and biases. Figure 3D shows the device's current-voltage characteristics, which are measured under different X-ray dose rates with bias sweeping from −20 to 20 V (see Figure S6a and Figure S6b for smaller voltage ranges). It is clearly shown that the measured device current rises upon the increase of X-ray dose rate throughout the whole operation voltages. For instance, at 20 V, the current changes from 0.19 nA in the dark to 0.65 nA at the X-ray dose rate of 3.1 μGy$_{air}$ s^{-1}, more than 200% enhancement, which reached 2.47 nA at the X-ray dose rate of 121.7 μGy$_{air}$ s^{-1}. The X-ray detection sensitivity of the device was evaluated at different operation voltages (5, 10, and 20 V). As shown in Figure 4A, the sensitivity was extracted from the plots of current density vs X-ray dose rate at different voltages by using eq 3

$$S = \frac{(J_{X-ray} - J_{dark})}{D} \tag{3}$$

where S represents the sensitivity, J_{X-ray} and J_{dark} represent the photocurrent and dark current densities, respectively, and D is the dose rate of X-ray. A sensitivity of 681 μC Gy$_{air}^{-1}$ cm^{-2} is achieved for the device at 5 V, which increases to 1,352 μC Gy$_{air}^{-1}$ cm^{-2} at 10 V and 2,292 μC Gy$_{air}^{-1}$ cm^{-2} at 20 V (Figure 4B). These values of X-ray detection sensitivity are indeed higher than that of commercially available detectors based on amorphous selenium (~22 μC Gy$_{air}^{-1}$ cm^{-2}).[16] Next, the limit of detection (LOD), one of the essential characteristics of radiation detectors for medical diagnostics and imaging applications,[17,28] was determined for the device by

https://doi.org/10.1021/acsenergylett.4c02662
ACS Energy Lett. 2024, 9, 5704−5711

taking multiple measurements within the region of low X-ray dose rates from 16 nGy_{air} s^{-1} to 60 nGy_{air} s^{-1} at 20 V (an electric field of 16.7 $V{\cdot}mm^{-1}$). According to the International Union of Pure and Applied Chemistry (IUPAC), the LOD is defined as the dose rate at a signal-to-noise ratio (SNR) of around 3, and for our device, the LOD is estimated to be 37.5 nGy_{air} s^{-1}, with an SNR value of 3.36, as shown in Figure 4C. This LOD value is about 150 times lower than the X-ray dose rate of 5.5 μGy_{air} s^{-1} required for standard medical diagnostics.[11] Note that the detection limit measurement was conducted with a current meter without additional signal filters in the circuit. With a more delicate electrical circuit design to filter out high-frequency noises, one would expect a better SNR and, thus, even lower LOD.

Finally, we investigated the operational stability of the 0D OMHH devices. We first stressed our detector under continuous X-ray irradiation with a dose rate of 178.7 μGy_{air} s^{-1} and at 20 V driving voltage for 24 h in ambient air with a relative humidity of around 35%. The time evolution of the X-ray-induced current is shown in Figure S7. It can be seen that the X-ray response of the device remains largely unchanged even after being exposed to an accumulative total dosage of 15, 440 mGy_{air} of X-ray. Next, we cycled our detector by turning the X-ray beam on and off periodically with a 20 s interval and monitored the X-ray-induced current from the detector. The X-ray dosage was kept at 178.7 μGy_{air} s^{-1} dose rate. As shown in Figure 4D, the device exhibits little-to-no drift in X-ray response after more than 580 continuous cycles. We further evaluated the long-term stability of the detector. Figure S8a shows that the device maintained stable and linear X-ray detection sensitivity at 20 V even 6 months after initial testing. At the same time, Figure S8b confirms there was almost no change in sensitivity upon retesting after 6 months. These findings underscore the superior stability of the device and highlight the potential of 0D OMHHs for practical radiological applications, where long-term stability is essential.

In summary, we report a new semiconducting 0D organic metal halide hybrid $(TPA\text{-}P)_2ZnBr_4$ for the fabrication of high-performance direct X-ray detectors, which exhibit a detection sensitivity of 2,292 μC Gy_{air}^{-1} cm^{-2} at 20 V with a low detection limit of 37.5 nGy_{air} s^{-1}. The direct X-ray detection using 0D $(TPA\text{-}P)_2ZnBr_4$ involves efficient molecular sensitization, where large bandgap metal halide species $ZnBr_4^{2-}$ act as X-ray absorber and organic semiconducting cations $TPA\text{-}P^+$ as charge transporter. The direct X-ray detectors have also shown superior long-term operational stability while being tested under a high dosage of accumulated X-ray irradiation at 20 V. The combination of low-cost facile preparation of the material, high detection sensitivity, low detection limit, and superior stability make direct X-ray detectors based on 0D organic metal halide hybrids highly promising for many practical applications, ranging from medical diagnostics to imaging, therapy, security, and scientific elucidations. This work again shows the exceptional structural tunability and rich functionalities of 0D organic metal halide hybrids with potential applications across a wide range of areas.

■ ASSOCIATED CONTENT

Supporting Information

The Supporting Information is available free of charge at https://pubs.acs.org/doi/10.1021/acsenergylett.4c02662.

Additional experimental details, synthesis, crystal growth, structural, optical, and electrochemical characterizations, and X-ray detector characterizations/calculations (PDF)

■ AUTHOR INFORMATION

Corresponding Authors

Wanyi Nie − *Department of Physics, University at Buffalo, Buffalo, New York 14260, United States;* orcid.org/0000-0002-5909-3155; Email: wanyinie@buffalo.edu

Biwu Ma − *Department of Chemistry and Biochemistry, Florida State University, Tallahassee, Florida 32306, United States;* orcid.org/0000-0003-1573-8019; Email: bma@fsu.edu

Authors

Oluwadara J. Olasupo − *Department of Chemistry and Biochemistry, Florida State University, Tallahassee, Florida 32306, United States*

Thanh-Hai Le − *Los Alamos National Laboratory, Los Alamos, New Mexico 87545, United States*

Tunde B. Shonde − *Department of Chemistry and Biochemistry, Florida State University, Tallahassee, Florida 32306, United States*

He Liu − *Department of Chemistry and Biochemistry, Florida State University, Tallahassee, Florida 32306, United States*

Alexander Bouchard − *Department of Chemistry and Biochemistry, Florida State University, Tallahassee, Florida 32306, United States*

Sara Bouchard − *Department of Chemistry and Biochemistry, Florida State University, Tallahassee, Florida 32306, United States*

Thilina N. D. D. Gamaralalage − *Department of Chemistry and Biochemistry, Florida State University, Tallahassee, Florida 32306, United States*

Abiodun M. Adewolu − *Department of Chemistry and Biochemistry, Florida State University, Tallahassee, Florida 32306, United States*

Tarannuma F. Manny − *Department of Chemistry and Biochemistry, Florida State University, Tallahassee, Florida 32306, United States*

Xinsong Lin − *Department of Chemistry and Biochemistry, Florida State University, Tallahassee, Florida 32306, United States*

Yan-Yan Hu − *Department of Chemistry and Biochemistry, Florida State University, Tallahassee, Florida 32306, United States*

Complete contact information is available at: https://pubs.acs.org/10.1021/acsenergylett.4c02662

Notes

The authors declare the following competing financial interest(s): O.J.O. and B.M. have filed a provisional patent application entitled Direct X-ray Detectors Based on Organic Metal Halide Hybrids to the United States Patent and Trademark Office (application # 63/677,634) on July 31, 2024.

■ ACKNOWLEDGMENTS

The authors acknowledge the funding support from the National Science Foundation (NSF) (DMR- 2204466) and the Florida State University Commercialization Investment

Program. This work used the Rigaku Synergy-S single-crystal X-ray diffractometer, acquired through the NSF MRI program (CHE-1828362). A portion of this work used resources provided by the X-ray Crystallography Center (FSU075000X-RAY) and the Materials Characterization Laboratory (FSU075000MAC) at the FSU Department of Chemistry and Biochemistry. W.N. acknowledges the funding support from the research foundation of the State University of New York, University at Buffalo. T.N.D.D.G. and Y.-Y.H. acknowledge the support from NSF under grant no. DMR-1847038. This work was performed, in part, at the Center for Integrated Nanotechnologies, an Office of Science User Facility operated for the U.S. Department of Energy (DOE) Office of Science. Los Alamos National Laboratory, an affirmative action-equal opportunity employer, is managed by Triad National Security, LLC for the U.S. Department of Energy's NNSA, under contract 89233218CNA000001. The authors thank Bill Stoffel for helping with the X-ray detector holder and Forrest Perry and Amy Allen for X-ray tube calibration.

REFERENCES

(1) Kotzur, I. WC Röntgen: a new type of ray. *Radiology* **1994**, *193* (2), 329−332.
(2) Kasap, S. O.; Rowlands, J. A. Direct-conversion flat-panel X-ray image sensors for digital radiography. *Proc. IEEE* **2002**, *90* (4), 591−604.
(3) Yakunin, S.; Sytnyk, M.; Kriegner, D.; Shrestha, S.; Richter, M.; Matt, G. J.; Azimi, H.; Brabec, C. J.; Stangl, J.; Kovalenko, M. V.; et al. Detection of X-ray photons by solution-processed lead halide perovskites. *Nat. Photonics* **2015**, *9* (7), 444−449.
(4) Tegze, M.; Faigel, G. X-ray holography with atomic resolution. *Nature* **1996**, *380* (6569), 49−51.
(5) Woodford, C.; Ashby, P., Non-destructive testing and radiation in industry. In *Fourth Conf. on Nuclear Science and Engineering in Australia*, 2001; Vol. *2001* Conf. handbook, Australia 198, pp 98−100.
(6) He, Y.; Song, J.; Li, M.; Sakhatskyi, K.; Li, W.; Feng, X.; Yang, B.; Kovalenko, M.; Wei, H. Perovskite computed tomography imager and three-dimensional reconstruction. *Nat. Photonics* **2024**, *18*, 1052−1058.
(7) Zhao, W.; Rowlands, J. A. X-ray imaging using amorphous selenium: Feasibility of a flat panel self-scanned detector for digital radiology. *Med. Phys.* **1995**, *22* (10), 1595−1604.
(8) Heiss, W.; Brabec, C. Perovskites target X-ray detection. *Nat. Photonics* **2016**, *10* (5), 288−289.
(9) Kasap, S.; Frey, J. B.; Belev, G.; Tousignant, O.; Mani, H.; Greenspan, J.; Laperriere, L.; Bubon, O.; Reznik, A.; DeCrescenzo, G.; et al. Amorphous and polycrystalline photoconductors for direct conversion flat panel X-ray image sensors. *Sensors* **2011**, *11*, 5112−5157.
(10) Stoumpos, C. C.; Malliakas, C. D.; Peters, J. A.; Liu, Z.; Sebastian, M.; Im, J.; Chasapis, T. C.; Wibowo, A. C.; Chung, D. Y.; Freeman, A. J.; et al. Crystal growth of the perovskite semiconductor CsPbBr3: a new material for high-energy radiation detection. *Cryst. Growth Des.* **2013**, *13* (7), 2722−2727.
(11) Wei, H.; Fang, Y.; Mulligan, P.; Chuirazzi, W.; Fang, H.-H.; Wang, C.; Ecker, B. R.; Gao, Y.; Loi, M. A.; Cao, L.; et al. Sensitive X-ray detectors made of methylammonium lead tribromide perovskite single crystals. *Nat. Photonics* **2016**, *10* (5), 333−339.
(12) Wei, W.; Zhang, Y.; Xu, Q.; Wei, H.; Fang, Y.; Wang, Q.; Deng, Y.; Li, T.; Gruverman, A.; Cao, L.; et al. Monolithic integration of hybrid perovskite single crystals with heterogenous substrate for highly sensitive X-ray imaging. *Nat. Photonics* **2017**, *11* (5), 315−321.
(13) Di, J.; Li, H.; Chen, L.; Zhang, S.; Hu, Y.; Sun, K.; Peng, B.; Su, J.; Zhao, X.; Fan, Y.; et al. Low trap density para-F substituted 2D PEA2PbX4 (X= Cl, Br, I) single crystals with tunable optoelectrical properties and high sensitive x-ray detector performance. *Research* **2022**, *2022*, No. 9768019.
(14) Wang, B.; Yang, X.; Li, R.; Qaid, S. M.; Cai, W.; Xiao, H.; Zang, Z. One-dimensional CsCu2I3 single-crystal X-ray detectors. *ACS Energy Lett.* **2023**, *8* (10), 4406−4413.
(15) Liu, Y.; Xu, Z.; Yang, Z.; Zhang, Y.; Cui, J.; He, Y.; Ye, H.; Zhao, K.; Sun, H.; Lu, R.; et al. Inch-size 0D-structured lead-free perovskite single crystals for highly sensitive stable X-ray imaging. *Matter* **2020**, *3* (1), 180−196.
(16) Kasap, S. X-ray sensitivity of photoconductors: application to stabilized a-Se. *J. Phys. D: Appl. Phys.* **2000**, *33* (21), 2853.
(17) Pan, W.; Wu, H.; Luo, J.; Deng, Z.; Ge, C.; Chen, C.; Jiang, X.; Yin, W.-J.; Niu, G.; Zhu, L.; et al. Cs2AgBiBr6 single-crystal X-ray detectors with a low detection limit. *Nat. photonics* **2017**, *11* (11), 726−732.
(18) Wei, H.; DeSantis, D.; Wei, W.; Deng, Y.; Guo, D.; Savenije, T. J.; Cao, L.; Huang, J. Dopant compensation in alloyed CH3NH3PbBr3− x Cl x perovskite single crystals for gamma-ray spectroscopy. *Nat. Mater.* **2017**, *16* (8), 826−833.
(19) Wei, H.; Huang, J. Halide lead perovskites for ionizing radiation detection. *Nat. Commun.* **2019**, *10* (1), 1066.
(20) Lin, Y.; Bai, Y.; Fang, Y.; Wang, Q.; Deng, Y.; Huang, J. Suppressed ion migration in low-dimensional perovskites. *ACS Energy Lett.* **2017**, *2* (7), 1571−1572.
(21) Xu, X.; Qian, W.; Xiao, S.; Wang, J.; Zheng, S.; Yang, S. Halide perovskites: A dark horse for direct X-ray imaging. *EcoMat* **2020**, *2* (4), No. e12064.
(22) Koenraad, P. M.; Flatté, M. E. Single dopants in semiconductors. *Nat. Mater.* **2011**, *10* (2), 91−100.
(23) Peng, W.; Yin, J.; Ho, K.-T.; Ouellette, O.; De Bastiani, M.; Murali, B.; El Tall, O.; Shen, C.; Miao, X.; Pan, J.; et al. Ultralow self-doping in two-dimensional hybrid perovskite single crystals. *Nano Lett.* **2017**, *17* (8), 4759−4767.
(24) Wang, Q.; Shao, Y.; Xie, H.; Lyu, L.; Liu, X.; Gao, Y.; Huang, J. Qualifying composition dependent p and n self-doping in CH3NH3PbI3. *Appl. Phys. Lett.* **2014**, *105* (16), No. 163508.
(25) Boyd, C. C.; Cheacharoen, R.; Leijtens, T.; McGehee, M. D. Understanding degradation mechanisms and improving stability of perovskite photovoltaics. *Chem. rev.* **2019**, *119* (5), 3418−3451.
(26) Christians, J. A.; Miranda Herrera, P. A.; Kamat, P. V. Transformation of the excited state and photovoltaic efficiency of CH3NH3PbI3 perovskite upon controlled exposure to humidified air. *J. Am. Chem. Soc.* **2015**, *137* (4), 1530−1538.
(27) Habisreutinger, S. N.; Leijtens, T.; Eperon, G. E.; Stranks, S. D.; Nicholas, R. J.; Snaith, H. J. Carbon nanotube/polymer composites as a highly stable hole collection layer in perovskite solar cells. *Nano Lett.* **2014**, *14* (10), 5561−5568.
(28) Zhuang, R.; Wang, X.; Ma, W.; Wu, Y.; Chen, X.; Tang, L.; Zhu, H.; Liu, J.; Wu, L.; Zhou, W.; et al. Highly sensitive X-ray detector made of layered perovskite-like (NH4) 3Bi2I9 single crystal with anisotropic response. *Nat. Photonics* **2019**, *13* (9), 602−608.
(29) Xiao, X.; Dai, J.; Fang, Y.; Zhao, J.; Zheng, X.; Tang, S.; Rudd, P. N.; Zeng, X. C.; Huang, J. Suppressed ion migration along the in-plane direction in layered perovskites. *ACS Energy Lett.* **2018**, *3* (3), 684−688.
(30) Li, W.; Li, M.; He, Y.; Song, J.; Guo, K.; Pan, W.; Wei, H. Arising 2D Perovskites for Ionizing Radiation Detection. *Adv. Mater.* **2024**, *36*, No. 2309588.
(31) Zhou, C.; Lin, H.; Tian, Y.; Yuan, Z.; Clark, R.; Chen, B.; van de Burgt, L. J.; Wang, J. C.; Zhou, Y.; Hanson, K.; et al. Luminescent zero-dimensional organic metal halide hybrids with near-unity quantum efficiency. *Chem. Sci.* **2018**, *9* (3), 586−593.
(32) He, Q.; Zhou, C.; Xu, L.; Lee, S.; Lin, X.; Neu, J.; Worku, M.; Chaaban, M.; Ma, B. Highly stable organic antimony halide crystals for X-ray scintillation. *ACS Mater. Lett.* **2020**, *2* (6), 633−638.
(33) Shonde, T. B.; Chaaban, M.; Liu, H.; Olasupo, O. J.; Ben-Akacha, A.; Gonzalez, F. G.; Julevich, K.; Lin, X.; Winfred, J. R. V.; Stand, L. M.; et al. Molecular sensitization enabled high performance organic metal halide hybrid scintillator. *Adv. Mater.* **2023**, *35* (23), No. 2301612.

https://doi.org/10.1021/acsenergylett.4c02662
ACS Energy Lett. 2024, 9, 5704−5711

(34) Shonde, T. B.; Mondal, A.; Liu, H.; Chaaban, M.; Ben-Akacha, A.; Lee, S.; Knorr, E. S.; Ma, B. Dramatically enhanced X-ray scintillation of BODIPY via sensitization by an organic metal halide. *ACS Mater. Lett.* **2022**, *4* (2), 271−276.
(35) Xu, L.-J.; Lin, X.; He, Q.; Worku, M.; Ma, B. Highly efficient eco-friendly X-ray scintillators based on an organic manganese halide. *Nat. Commun.* **2020**, *11* (1), 4329.
(36) You, S.; Zhu, Z. K.; Dai, S.; Wu, J.; Guan, Q.; Zhu, T.; Yu, P.; Chen, C.; Chen, Q.; Luo, J. Inch-Size Single Crystals of Lead-Free Chiral Perovskites with Bulk Photovoltaic Effect for Stable Self-Driven X-Ray Detection. *Adv. Funct. Mater.* **2023**, *33* (36), No. 2303523.
(37) Thirimanne, H.; Jayawardena, K.; Parnell, A.; Bandara, R.; Karalasingam, A.; Pani, S.; Huerdler, J.; Lidzey, D.; Tedde, S.; Nisbet, A.; et al. High sensitivity organic inorganic hybrid X-ray detectors with direct transduction and broadband response. *Nat. Commun.* **2018**, *9* (1), 2926.
(38) Li, H.; Shan, X.; Neu, J. N.; Geske, T.; Davis, M.; Mao, P.; Xiao, K.; Siegrist, T.; Yu, Z. Lead-free halide double perovskite-polymer composites for flexible X-ray imaging. *Journal of Materials Chemistry C* **2018**, *6* (44), 11961−11967.
(39) Tsai, H.; Liu, F.; Shrestha, S.; Fernando, K.; Tretiak, S.; Scott, B.; Vo, D. T.; Strzalka, J.; Nie, W. A sensitive and robust thin-film x-ray detector using 2D layered perovskite diodes. *Sci. Adv.* **2020**, *6* (15), No. eaay0815.
(40) Zhang, Y.; Liu, Y.; Xu, Z.; Ye, H.; Yang, Z.; You, J.; Liu, M.; He, Y.; Kanatzidis, M. G.; Liu, S. Nucleation-controlled growth of superior lead-free perovskite Cs3Bi2I9 single-crystals for high-performance X-ray detection. *Nat. Commun.* **2020**, *11* (1), 2304.
(41) Peng, J.; Xia, C. Q.; Xu, Y.; Li, R.; Cui, L.; Clegg, J. K.; Herz, L. M.; Johnston, M. B.; Lin, Q. Crystallization of CsPbBr3 single crystals in water for X-ray detection. *Nat. Commun.* **2021**, *12* (1), 1531.
(42) Feng, Y.; Pan, L.; Wei, H.; Liu, Y.; Ni, Z.; Zhao, J.; Rudd, P. N.; Cao, L. R.; Huang, J. Low defects density CsPbBr 3 single crystals grown by an additive assisted method for gamma-ray detection. *J. Mater. Chem.* **2020**, *8* (33), 11360−11368.
(43) Berger, M. XCOM: photon cross sections database. https://physics.nist.gov/PhysRefData/FFast/html/form.html (accessed 10/21/24).
(44) Reyes-Retana, J.; Valladares, A. A. Structural properties of amorphous selenium: An ab initio molecular-dynamics simulation. *Comput. Mater. Sci.* **2010**, *47* (4), 934−939.
(45) Yang, B.; Pan, W.; Wu, H.; Niu, G.; Yuan, J.-H.; Xue, K.-H.; Yin, L.; Du, X.; Miao, X.-S.; Yang, X.; et al. Heteroepitaxial passivation of Cs2AgBiBr6 wafers with suppressed ionic migration for X-ray imaging. *Nat. Commun.* **2019**, *10* (1), 1989.
(46) Leijtens, T.; Hoke, E. T.; Grancini, G.; Slotcavage, D. J.; Eperon, G. E.; Ball, J. M.; De Bastiani, M.; Bowring, A. R.; Martino, N.; Wojciechowski, K.; et al. Mapping electric field-induced switchable poling and structural degradation in hybrid lead halide perovskite thin films. *Adv. Energy Mater.* **2015**, *5* (20), No. 1500962.

https://doi.org/10.1021/acsenergylett.4c02662
ACS Energy Lett. 2024, 9, 5704−5711